The Astrophysical Journal, 971:145 (7pp), 2024 August 20 https://doi.org/10.3847/1538-4357/ad5ff5
© 2024. The Author(s). Published by the American Astronomical Society.
OPEN ACCESS

# Testing General Relativity with Juno at Jupiter

Daniele Durante[1], P. Cappuccio[1], I. di Stefano[1], M. Zannoni[2], L. Gomez Casajus[2], G. Lari[3], M. Falletta[3], D. R. Buccino[4], L. Iess[1], R. S. Park[4], and S. J. Bolton[5]
[1] Department of Mechanical and Aerospace Engineering, Sapienza University of Rome, Italy; daniele.durante@uniroma1.it
[2] Department of Industrial Engineering, University of Bologna, Forlì, Italy
[3] Department of Mathematics, University of Pisa, Italy
[4] Jet Propulsion Laboratory, California Institute of Technology, Pasadena, CA, USA
[5] Southwest Research Institute, San Antonio, TX, USA
*Received 2024 June 12; accepted 2024 July 5; published 2024 August 14*

## Abstract

The Juno spacecraft has been orbiting Jupiter since 2016 July to deepen our comprehension of the solar system by studying the gas giant. The radio science experiment enables the determination of Jupiter's gravitational field, thus shedding light on its interior structure. The experiment relies on determining the orbit of the spacecraft during its pericenter passages. Previous gravity data analyses assumed the correctness of the general theory of relativity, which was used for trajectory integration and radio signal propagation modeling. In this work, we aim to test general relativity within the unique context of a spacecraft orbiting Jupiter, by employing the parameterized post-Newtonian (PPN) formalism, an established framework for comparing various gravitational theories. Within this framework, we focus our attention toward the PPN parameters $\gamma$ and $\beta$, which offer insights into the curvature of spacetime and the nonlinearity of gravitational effects, respectively. Additionally, we extend our investigation to the Lense–Thirring effect, which models the dragging of spacetime induced by a rotating mass. By measuring the relativistic frequency shift on Doppler observables caused by Jupiter during Juno's perijove passes, we estimate $\gamma = 1 + (1.5 \pm 4.9) \times 10^{-3}$, consistent with the general theory of relativity. Our estimated $\gamma$ is primarily influenced by its effect on light-time computation, with a negligible contribution from spacecraft dynamics. Furthermore, we also present a modest level of accuracy for the $\beta$ parameter, reflecting the minimal dynamical perturbation on Juno from general relativity. This also applies to the Lense–Thirring effect, whose signal is too small to be confidently resolved.

*Unified Astronomy Thesaurus concepts:* Jupiter (873); General relativity (641); Orbit determination (1175)

## 1. Introduction

The NASA Juno spacecraft is orbiting Jupiter since 2016 July to improve our knowledge of the solar system by understanding the origin and evolution of the planet (Bolton et al. 2017). Given the high-eccentricity orbits, the spacecraft flies very close to Jupiter, experiencing the large gravitational field of the gas giant. The radio science instrumentation on board Juno enabled accurate determination of the gravity acceleration exerted by Jupiter, revealing the north–south asymmetry of the field (Iess et al. 2018; Durante et al. 2020), as well as determining characteristic features, such as the effect of the Great Red Spot (Parisi et al. 2021) or that of normal modes (Durante et al. 2022). All the previous analyzes of Juno gravity data assumed, very reasonably, the correctness of the general theory of relativity (Einstein 1915, 1916), which is used both for the computation of the Juno trajectory and for modeling of the propagation of radio signals sent back and forth between the spacecraft and the ground station. In this work, we aim to test the general theory of relativity for a spacecraft around Jupiter.

To test and compare gravitational theories in the solar system, the parameterized post-Newtonian (PPN) formalism is often used as an effective framework (Will 2014, 2018). This formalism leverages on a series expansion of the spacetime metric, introducing 10 parameters that multiply each term of the expansion. These parameters have a specific physical meaning, and they assume a fixed value that depends on the considered gravitational theory.

The PPN parameter $\gamma$ describes the spacetime curvature produced by any mass distribution, and, consequently, controls the deflection of light caused by massive bodies. According to the general theory of relativity, its value is equal to 1; thus any measured deviation from this prediction entails a violation of the theory. All previous experiments aimed at constraining the value of $\gamma$ were meant to measure the effects on radiometric data caused by the spacetime curvature induced by the mass of the Sun. The most accurate estimate of $\gamma = 1 + (2.1 \pm 2.3) \times 10^{-5}$ was provided by measurements carried out in 2002, during a solar conjunction of the spacecraft Cassini in the cruise phase to Saturn (Bertotti et al. 2003). Given the vicinity of the link to the Sun and thus to the solar corona (full of charged particles), multifrequency links are mandatory to produce accurate radiometric measurements with this experiment configuration. So far, Jupiter has also been exploited to test general relativity. By using the solar system largest planet as a gravitational lens, the deflection of light coming from distant sources can be measured to test gravitational theories. By measuring the light deflection of quasars via the Very Long Baseline Array technique (experiment detailed in Fomalont & Kopeikin 2003), Fomalont & Kopeikin (2007) reported a value for the $\gamma$ parameter of $1.01 \pm 0.03$. More recently, the measure of relative positions between two pairs of compact extragalactic sources enabled another accurate determination of $\gamma$, resulted to be $0.984 \pm 0.037$ (Li et al. 2022).

Original content from this work may be used under the terms of the Creative Commons Attribution 4.0 licence. Any further distribution of this work must maintain attribution to the author(s) and the title of the work, journal citation and DOI.

Although the constraint on $\gamma$ obtained by Cassini during the solar conjunction experiment is significantly tighter, these tests have been performed by measuring the relativistic light deflection caused by Jupiter, rather than the Sun. With Juno we can test general relativity at Jupiter, thus in a different environment from that of previous experiments performed via radio tracking of a cooperating spacecraft. Note that contrary to the Sun, where the plasma noise induced by the solar corona limits the minimum impact parameter of the link obtainable via radio tracking, Jupiter does not present this limitation, thus providing an optimal configuration for this type of experiment.

The PPN parameter $\beta$ is related to the nonlinearity in the superposition law for gravity, and its value is one according to general relativity. Experimental verifications aimed at the estimate of this parameter have been carried out by means of global fits of optical and radio data for the construction of planetary ephemeris, such as with the Intégrateur Numérique Planétarie de l'Observatorie de Paris (INPOP) software, which resulted in an accuracy on the $\beta$ parameter at level of $7 \times 10^{-5}$ (Fienga et al. 2015). More recently, Park et al. (2017) analyzed range data of the MESSENGER spacecraft in orbit about Mercury to estimate the precession of Mercury's perihelion, which is linked to a linear combination of $\beta$ and $\gamma$. This analysis provided the estimate $\beta = 1 + (-2.7 \pm 3.9) \times 10^{-5}$.

In this work, we aim to test general relativity with the Doppler data collected by Juno while orbiting Jupiter. This is the first time that a cooperating spacecraft is used to test relativistic gravity by measuring the light deflection caused by a body different from the Sun. Our experiment is not limited to measuring the PPN parameters $\beta$ and $\gamma$, but given the close proximity of Juno to Jupiter the spacecraft dynamics is also influenced by the Lense–Thirring effect. This is a relativistic secular precession of both the longitude of the ascending node and the argument of perihelion of the spacecraft produced by the nonzero angular momentum of the central body. Ciufolini et al. (2019) verified the Lense–Thirring effect on the R.A. of the ascending node for the LAGEOS 1, LAGEOS-2, and LARES satellites orbiting around the Earth with a precision of 2%. The motion of Mercury's orbit is also shown to be influenced by the Lense–Thirring effect (Park et al. 2017). A significant improvement is expected with data from the LARES 2 satellite, which may allow a test of frame-dragging with an uncertainty as small as a few parts in one thousand (Ciufolini et al. 2023).

This manuscript is structured as follows: Section 2 provides a description of the general relativity effects acting on Juno, Section 3 reports the orbit determination procedure used to analyze the data, Section 4 provides experiment results, and Section 5 gives comments and conclusions.

## 2. Effects of General Relativity on Juno

With the Juno spacecraft orbiting around Jupiter, general relativity plays different roles in shaping the orbit around the planet and in perturbing the radio signals sent back and forth between the spacecraft and the Earth. Since Jupiter is massive and Juno comes very close to its 1 bar surface (the perijove altitude was as low as 4000 km in given passes), the spacetime deformation induced by the planet is large.

We can distinguish between three main effects:

1. Relativistic time delay on the radio signals (accounting also for Jupiter oblateness);
2. Correction to Newtonian acceleration caused by general relativity (accounting also for Jupiter oblateness);
3. Lense–Thirring effect due to Jupiter's fast rotation speed.

The relativistic time delay (also known as the Shapiro time delay) and the consequent frequency shift must be accounted for when computing the expected value of radiometric measurements collected during Juno's close approach to Jupiter, whereas the second and third effects are a direct perturbation of the Juno orbit. The model for these effects are already included in JPL's orbit determination software, MONTE (Evans et al. 2018), which was used to analyze Juno radiometric data (see Section 3).

### 2.1. Relativistic Time Delay

One of the first experimental verification of the general theory of relativity has been made by observing the bending of light rays when passing nearby the Sun. The bending is caused by the Sun's strong gravitational field, which deforms the spacetime and thus the path of the light. However, in addition to bending, the light (or radio waves in general) passing through the gravitational field also experiences a time delay, called the Shapiro time delay (Shapiro 1964), which depends on the PPN $\gamma$ parameter. In the years following the discovery of the relativistic light deflection, several verifications of the effect of $\gamma$ have been performed exploiting radar measurements collected from targets during superior solar conjunctions (SSCs). These tests were initially carried out with passive targets like Mercury and Venus (Shapiro et al. 1968, 1971) and then with active spacecraft. Active spacecraft retransmitting the uplink signal back to the ground demonstrated to be a useful tool to measure the Shapiro time delay, as in the case of Mariner 6 and 7 (Anderson et al. 1975) and Vikings (Reasenberg et al. 1979). Currently, the most accurate determination of the $\gamma$ parameter comes from the solar conjunction experiment performed by the Cassini spacecraft (Bertotti et al. 2003), which resulted in $\gamma = 1 + (2.1 \pm 2.3) \times 10^{-5}$, confirming the general theory of relativity to outstanding accuracy. Similar experiments leveraging advanced radio tracking instrumentation have been performed with ESA's BepiColombo spacecraft (di Stefano et al. 2021) and have been proposed also in the context ESA's JUICE mission (di Stefano et al. 2022). The gravitational time delay formulation (Moyer 2008) implemented in MONTE for all the bodies is

$$\Delta t = \frac{(1+\gamma)GM}{c^3} \ln\left(\frac{r_1 + r_2 + r_{12} + \frac{(1+\gamma)GM}{c^2}}{r_1 + r_2 - r_{12} + \frac{(1+\gamma)GM}{c^2}}\right), \quad (1)$$

where $GM$ is the gravitational parameter of the massive body, $c$ is the speed of light, while $r_1$ and $r_2$ are the distance between the massive body and, respectively, the transmitter and the receiver, whereas $r_{12}$ is their relative distance. This approximates the full second-order expression of the gravitational time delay, whose complete formulation has been derived in Cappuccio et al. (2021) for the BepiColombo radio science experiment (Iess et al. 2021). However, as shown in Cappuccio et al. (2021), Equation (1) includes the second-order terms that are enhanced during SSCs, acting as a sufficiently accurate approximation for most of the test performed in the solar system. Note that the terms inside the logarithm proportional to $1/c^2$ (accounting for the bending of the signal path) are generally important only for the Sun, and this is the case also

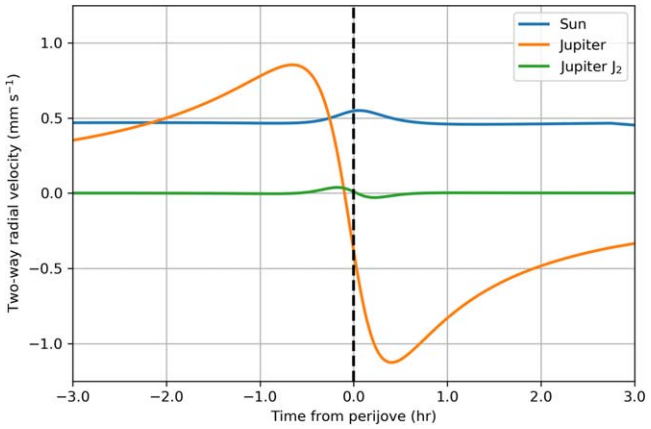


**Figure 1.** Relativistic frequency shift from the Sun, Jupiter, and its oblateness, expressed in terms of range rate on a typical perijove pass (PJ06). The vertical dashed line indicates the time of the closest approach.

for Juno at Jupiter, where the bending contribution coming from Jupiter is negligible (i.e., below the numerical precision). We verified that a full second order formulation is not required for the Juno case since the difference with respect to Equation (1) is negligible. This is also true for the gravitomagnetic effect caused by Jupiter angular momentum (see Ciufolini et al. 2003), which is orders of magnitudes below the noise level.

The relativistic effect on Juno's Doppler data during a typical perijove pass is shown in Figure 1. As a comparison, in the case of BepiColombo solar superior conjunction, the maximum path delay caused by the Sun on the two-way signal was 50 km on range data and 4.2 cm s$^{-1}$ in terms of radial velocity, corresponding to $1.4\times10^{-10}$ on the fractional frequency shift of the signal.

Since Jupiter's oblateness is significant, the spacetime surrounding the body is not spherically symmetric, and the light path gets distorted and delayed. Even if this effect is only a minor correction to the light-time computation, it has been included in our analysis. The additional correction is (Le Poncin-Lafitte & Teyssandier 2008)

$$\Delta t_{J_2}=\frac{(1+\gamma)GM}{2\,c^3}\,\frac{J_2R^2}{r_1r_2}\left\{\frac{r_{12}}{1+(\hat{r}_1\cdot\hat{r}_2)}\left[\frac{1-(\hat{z}\cdot\hat{r}_1)^2}{r_1}+\frac{1-(\hat{z}\cdot\hat{r}_2)^2}{r_2}-\left(\frac{1}{r_1}+\frac{1}{r_2}\right)\frac{[\hat{z}\cdot(\hat{r}_1+\hat{r}_2)]^2}{1+(\hat{r}_1\cdot\hat{r}_2)}\right]\right\}, \tag{2}$$

where $J_2$ is the unnormalized zonal harmonic coefficient of degree 2 (representing the oblateness, $J_2\sim0.0147$), $R$ is the reference radius of the spherical harmonics' expansion ($R=71{,}492$ km), and $\hat{z}$ is the body's rotational pole direction. Note that the Juno spacecraft fully experiences this effect along its polar orbit, since the perijoves are close to the equator (shifting northward over time), where the effect is at its maximum. Additionally, the fast motion near the perijove (velocities up to $\sim$60 km s$^{-1}$ at pericenter) increases the effect on the Doppler data. On PJ06, the additional two-way delay is of the order of a few centimeters, giving rise to a Doppler shift of up to 0.04 mm s$^{-1}$ (see Figure 1), several times the noise level at 60 s integration time. This is about 20 times smaller than the peak Doppler shift from Jupiter's monopole.

### 2.2. Acceleration due to General Relativity

The acceleration acting on the spacecraft in a general relativity framework is accounted for as a correction to the Newtonian dynamics via the post-Newtonian (PN) parameterization (Will 2014, 2018). Since it is included in the spacecraft dynamics as an additional acceleration with respect to the Newtonian acceleration, we will refer to this correction as the acceleration caused by general relativity. Being the effect of order $\sim v^2/c^2$, with $v$ the spacecraft velocity and $c$ the speed of light, such a correction is generally quite small, although not negligible on Juno given the large velocities reached when passing at the perijove. The acceleration acting on the spacecraft (subscript $p$) accounting for the relativistic effects due to the monopole term of the gravitational potentials of a set of bodies (subscript $i$) with respect to the barycenter of the solar system is given by the Einstein–Infeld–Hoffman equations:

$$\begin{aligned}\vec{a}_p=\sum_i\frac{GM_i}{r_{ip}^2}\Bigg[&-\frac{2(\gamma+\beta)}{c^2}\sum_j\frac{GM_j}{r_{jp}}-\frac{2\beta-1}{c^2}U_i+\frac{\gamma}{c^2}v_p^2\\&+\frac{\gamma+1}{c^2}v_i^2-\frac{2(\gamma+1)}{c^2}(\vec{v}_p\cdot\vec{v}_i)-\frac{3}{2c^2}\left(\frac{\vec{v}_i\cdot\vec{r}_{ip}}{r_{ip}}\right)^2\\&-\frac{(\vec{r}_{ip}\cdot\vec{a}_i)}{2c^2}\Bigg]\vec{r}_{ip}+\frac{1}{c^2}\sum_i\frac{GM_i}{r_{ip}^3}\{\vec{r}_{ip}\cdot[(2\gamma+2)\vec{v}_p\\&-(2\gamma+1)\vec{v}_i]\}\vec{v}_{ip}+\frac{4\gamma+3}{2c^2}\sum_i\frac{GM_i}{r_{ip}}\vec{a}_i.\end{aligned} \tag{3}$$

Then, the acceleration of the spacecraft with respect to the Jupiter system barycenter (i.e., our integration center, subscript $b$) is obtained by subtracting the inertial acceleration due to relativity acting on the Jupiter system barycenter, which is given by

$$\begin{aligned}\vec{a}_b=\sum_{i\neq b}\frac{GM_i}{r_{bi}^2}\Bigg[&-\frac{2(\gamma+\beta)}{c^2}\sum_{j\neq b}\frac{GM_j}{r_{bj}}-\frac{2\beta-1}{c^2}U_i+\frac{\gamma}{c^2}v_b^2\\&+\frac{\gamma+1}{c^2}v_i^2-\frac{2(\gamma+1)}{c^2}(\vec{v}_b\cdot\vec{v}_i)-\frac{3}{2c^2}\left(\frac{\vec{v}_i\cdot\vec{r}_{bi}}{r_{bi}}\right)^2\\&-\frac{(\vec{r}_{bi}\cdot\vec{a}_i)}{2c^2}\Bigg]\vec{r}_{bi}+\frac{1}{c^2}\sum_{i\neq b}\frac{GM_i}{r_{bi}^3}\{\vec{r}_{bi}\cdot[(2\gamma+2)\vec{v}_b\\&-(2\gamma+1)\vec{v}_i]\}\vec{v}_{bi}+\frac{4\gamma+3}{2c^2}\sum_i\frac{GM_i}{r_{bi}}\vec{a}_i.\end{aligned} \tag{4}$$

In the latter $\vec{a}_b$ term, the summations are done on the set of bodies, excluding these participating in the definition of the Jupiter system (i.e., Jupiter and its satellites). The potential $U_i$ at relativistic body $i$ due to all other bodies is defined as

$$U_i=\sum_{k\neq i}\frac{GM_k}{r_{ki}}. \tag{5}$$

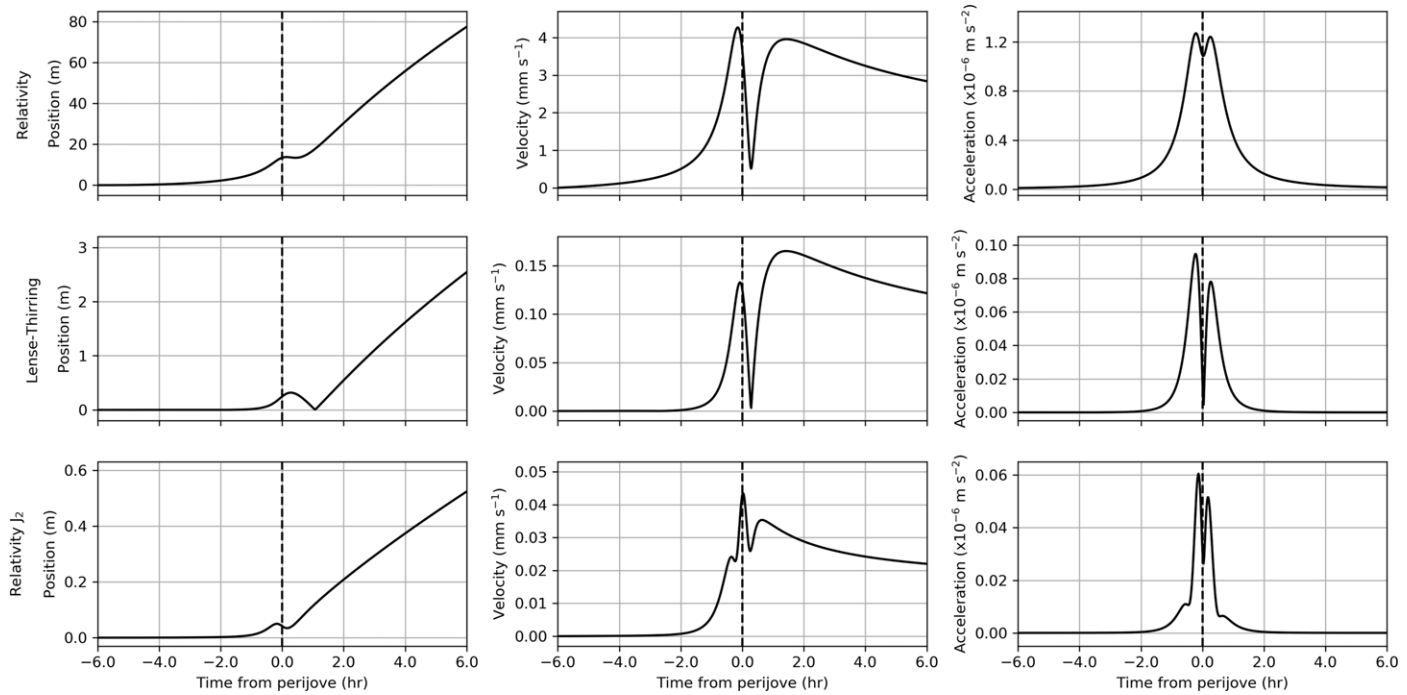


**Figure 2.** Effect on Juno position and velocity induced by the general relativity (top panels), Lense–Thirring (mid panels), and relativistic oblateness (bottom panels) accelerations, on a typical perijove pass (PJ03). The vertical dashed line indicates the time of the closest approach.

The acceleration $\overrightarrow{a_i}$ of a relativistic body $i$ can be approximated with the Newtonian acceleration due to all the other bodies:

$$\overrightarrow{a_i} = -\sum_{k \neq i} \frac{GM_k}{r_{ki}^3} \overrightarrow{r_{ki}}. \tag{6}$$

In the above equations, $\overrightarrow{r}$, $\overrightarrow{v}$, and $\overrightarrow{a}$ refer respectively to inertial position, velocity, and acceleration relative to the solar system barycenter, whereas $GM$ is the gravitational parameter of a body. The $\gamma$ and $\beta$ PPN parameters are generally used to test gravitation theories. General relativity predicts that their values are both equal to 1, thus measuring any deviations from unity would violate the theory.

The effect of relativistic acceleration acting on Juno (with respect to Newtonian dynamics) is reported in Figure 2 (top panels) for a typical perijove pass. Due to the nature of Juno's orbit, the largest acceleration occurs near the perijove, where the relativistic acceleration peaks at $\sim 10^{-6}\,\mathrm{m\,s^{-2}}$. As a comparison, the Newtonian peak acceleration due to Jupiter is $\sim 25\,\mathrm{m\,s^{-2}}$, the effect of its oblateness ($J_2$) is $\sim 0.45\,\mathrm{m\,s^{-2}}$, and the acceleration due to solar radiation pressure, the dominating nongravitational acceleration, is $\sim 6 \times 10^{-9}\,\mathrm{m\,s^{-2}}$ on average (Tommei et al. 2015; Notaro et al. 2021). The relativistic acceleration perturbs the Juno trajectory (position and velocity): in a time span of about 12 hr, the spacecraft velocity changes as much as $4\,\mathrm{mm\,s^{-1}}$, corresponding to a displacement of $\sim 80$ m. Note that the noise in radial velocity from radiometric Doppler data is about $0.01\,\mathrm{mm\,s^{-1}}$ at an integration time of 60 s (see Durante et al. 2020); thus this effect is several orders of magnitude larger than the data noise level.

Similarly to the case of the relativistic time delay, Jupiter's oblateness plays a role also in the relativistic acceleration. Jupiter's quadrupole zonal coefficient $J_2$ contributes to the relativistic acceleration, producing an additional term in the spacecraft dynamics (Soffel et al. 1988):

$$\begin{aligned}
&\overrightarrow{a}_{\mathrm{rel_}J_2} \\
&= \frac{GM}{c^2 r} J_2 \left(\frac{R}{r}\right)^2 \left\{ 2(\gamma+\beta) \left[ \left(2 - 9\frac{z^2}{r^2}\right) \frac{\overrightarrow{r}}{r} + 3\frac{z}{r}\hat{z} \right] \frac{GM}{r^2} \right. \\
&\quad + 3(\gamma+1) \left[ \left(1 - 5\frac{z^2}{r^2}\right) \frac{\overrightarrow{r}\cdot\overrightarrow{v}}{r} + 2\frac{z}{r} v_z \right] \frac{\overrightarrow{v}}{r} \\
&\quad \left. - \frac{3}{2}\gamma \left[ \left(1 - 5\frac{z^2}{r^2}\right) \frac{\overrightarrow{r}}{r} + 2\frac{z}{r}\hat{z} \right] \frac{v^2}{r} \right\},
\end{aligned} \tag{7}$$

where $z$ and $v_z$ are the position and velocity coordinates of the spacecraft along the $\hat{z}$ axis of the central body. Note that this acceleration is not included in the MONTE software and has been added separately. We compared our implementation against the ORBIT14 orbit determination code and found good agreement. Note that ORBIT14, contrary to MONTE, integrates the equation of motion in local spacetime coordinates, following a multichart approach (Serra et al. 2016, 2019; Lari et al. 2022).

The effect is $\sim 6 \times 10^{-8}\,\mathrm{m\,s^{-2}}$ at pericenter (see Figure 2, bottom panels), and relevant only when close to the planet. This is about a factor $\sim 20$ smaller than that coming from the relativistic acceleration caused by the monopole terms.

### 2.3. Lense–Thirring Effect

The Lense–Thirring effect, also known as frame-dragging or Lense–Thirring precession, is a consequence of the general theory of relativity which arises because a rotating massive object warps the surrounding spacetime not only due to its gravity, but also due to its rotation. The body rotation drags the local reference frame, causing a warping of the spacetime, which results in an additional acceleration from the point of

view of an orbiting spacecraft. The effect has been first predicted by Lense and Thirring in 1918 (Lense & Thirring 1918), and several tests of the theory has been made in recent years with the LAGEOS and LARES satellites around the Earth (e.g., Ciufolini & Pavlis 2004; Ciufolini et al. 2023, 2019), confirming general relativity predictions. Similar tests have been proposed on other planets, such as Jupiter (Helled et al. 2011) or Uranus (Iorio et al. 2023).

Testing the Lense–Thirring effect can provide another evidence in support of the validity of general relativity, highlighting the intricate interplay between mass, rotation, and spacetime. The acceleration caused on a spacecraft while orbiting a massive rotating body, i.e., the Lense–Thirring effect, is

$$\vec{a}_{\rm LT} = \frac{(1+\gamma)G}{c^2 r^3}\left[-\vec{J} + \frac{3(\vec{J}\cdot\vec{r})\,\vec{r}}{r^2}\right]\times\vec{v}, \qquad (8)$$

with $J$ being the angular momentum vector of the planet, and $\vec{r}$ and $\vec{v}$ the position and velocity vectors of the spacecraft with respect to the planet. To accurately compute the Lense–Thirring effect, it is important to know Jupiter orientation, i.e., the direction of its angular momentum in space. In general, the angular momentum is defined as $\vec{J} = I\,\vec{\omega}$, with $I$ the inertia matrix of the body and $\vec{\omega}$ the spin axis. Recent results from Juno gravity data analysis have shown that the off-diagonal inertia terms (associated to degree-2 tesseral coefficients) are small and statistically compatible with zero (e.g., Durante et al. 2020; Lari et al. 2024). In addition, we can also neglect the effect of tides and normal modes on the inertia matrix, being small effects. The associated misalignment between the principal polar axis of inertia and Jupiter's pole has been constrained to be smaller than 10 m. Thus, we can assume that Jupiter angular momentum, its pole, and spin axis remain aligned over time (see Lari et al. 2024 for further discussions). Under this simplifying assumption, the inertia matrix is diagonal and $\vec{\omega}$ only has a component along the body's pole, $\hat{z}$.

The angular momentum vector can be rewritten as

$$\vec{J} = (kMR^2)\omega\hat{z}, \qquad (9)$$

where $k$ represents the polar moment of inertia factor (or normalized moment of inertia, NMoI). This is the main parameter controlling the Lense–Thirring effect, being currently the one affected by the largest uncertainty. However, interior models predict small variations in the polar moment of inertia when changing assumptions on the interior structure within reasonable limits, with an accepted value of about $k = 0.264$ (e.g., Helled et al. 2011; Militzer & Hubbard 2023). Given the small variability in the predicted value with different interior models, we fix this parameter and look for deviation from the expected Lense–Thirring acceleration acting on Juno. Note that in principle the differential rotation of Jupiter's interior can modify the angular momentum magnitude. However, such effect produces a relative deviation of the order of $10^{-5}$ (Militzer & Hubbard 2023), and thus can be neglected in our analysis (it is orders of magnitude smaller than our final accuracy; see Table 1).

**Table 1**
Results for General Relativity Estimated Parameters

| Parameter | Estimated Value and $1\sigma$ Uncertainty |
|---|---|
| $\gamma$ | $1.0015 \pm 0.0049$ |
| $\gamma$ (only from time delay) | $1.0014 \pm 0.0049$ |
| $\beta$ | $1.069 \pm 0.078$ |
| LT | $0.67 \pm 0.67$ |

**Note.** The theory predicts a value of 1 for these parameters.

Figure 2 (mid panels) reports the acceleration due to the Lense–Thirring effect and its influence on position and velocity during a typical Juno pass. The peak acceleration is $\sim 10^{-7}\,\mathrm{m\,s^{-2}}$, about 10 times smaller than that due to general relativity. The spacecraft velocity changes as much as $0.15\,\mathrm{mm\,s^{-1}}$ whereas the position deviates by about 3 m after 12 hr. That is, the effect is very small, and we can expect it will be difficult to be measured by Juno.

## 3. Orbit Determination of Juno

The orbit determination of Juno and tests of general relativity have been performed by analyzing Doppler data with JPL's MONTE software (Evans et al. 2018). Our analysis includes Juno gravity-dedicated passes up to PJ33 (the Prime Mission data set, used by Durante et al. 2022), for a total of 22 passes, with the addition of 4 more passes performed during the Extended Mission (PJ35, PJ41, PJ47, and PJ54) supported by *Ka*-band uplink. Note that in the Prime Mission the $Ka/Ka$ link (which requires the Goldstone complex from NASA Deep Space Network, DSN) was established in most of the gravity-dedicated passes, whereas such constrain was relaxed during the Extended Mission. That is, most of the passes executed during the Extended Mission were supported only by $X/X$ and $X/Ka$ links, from different DSN complexes, which provides, on average, inferior data quality. Concerning data calibration, when $Ka/Ka$ (or $X/Ka$) data were available in addition to the $X/X$ data, multifrequency link calibrations were applied to reduce dispersive noise (Mariotti & Tortora 2013). Advanced Water Vapor Radiometer (AWVR) data were also used (when available) to accurately calibrate the data from fluctuations induced by Earth troposphere (Buccino et al. 2021). Note that the AWVR radiometer is installed at the Goldstone complex; thus such an accurate calibration is only available in passes supported by that complex, which are usually the same passes with Ka-band uplink data.

Similarly to previous analysis of Juno's Doppler data (e.g., Folkner et al. 2017; Iess et al. 2018; Durante et al. 2020, 2022; Kaspi et al. 2023), the spacecraft dynamical model accounts for the gravitational accelerations of solar system planets, Jupiter and its satellites, in a relativistic 1-PN framework; the gravitational tides raised by the Sun and Galilean satellites on Jupiter; the motion of Jupiter's spin axis in the plane of the sky; the nongravitational accelerations caused by solar radiation pressure, Jupiter's albedo and infrared emission, and the anisotropic thermal acceleration caused by solar panels' difference in temperature. The aspherical gravity field of Jupiter is modeled via an expansion in spherical harmonics. The motion of planets and satellites are modeled using DE440 (Park et al. 2021) and JUP380.

The Doppler data acquired during the perijove passes have been analyzed via a multiarc least squares estimation filter. For

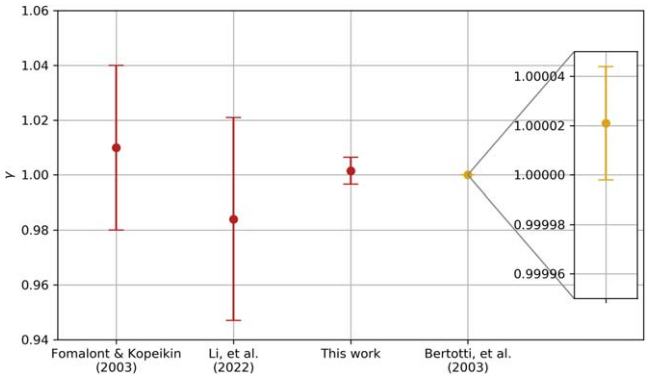


**Figure 3.** Comparison between our estimate of the $\gamma$ parameter with the previous estimates obtained at Jupiter (in red) and the most accurate result obtained with the Sun (in yellow). The uncertainty ($1\sigma$) of our solution is a factor of $\sim$4 smaller than previous results at Jupiter.

each perijove pass, we solve for the following (local parameters): Juno's initial position and velocity, the velocity change during Earth repointing turns (if any), and empirical piecewise constant accelerations (updating every 4 minutes in a 2 hr timeframe centered about the perijove pass). These accelerations are used to account for possible mismodeling in Juno dynamical model, caused for example by Jupiter's normal modes (Durante et al. 2022), which we do not account for. The choice of using empirical accelerations instead of a different model is for simplify the data analysis while retaining all important effects. However, we tested solutions including normal modes and obtained statistically compatible results. The parameters common to all arcs (i.e., global) are as follows: Jupiter's gravitational parameter (GM), zonal harmonic coefficients to degree 40, tesseral coefficients of degree-2 (included to look for a possible misalignment between the polar axis of inertia and Jupiter spin axis, and equatorial ellipticity), Jupiter's tidal Love numbers up to degree and order 4 (equal among satellites), Jupiter's spin axis initial position, polar moment of inertia factor, a scale factor for the Lense–Thirring effect (nominal value of 1), the mass associated to the Great Red Spot dipolar structure, the PPN parameters $\gamma$ and $\beta$, and a scale factor for the solar radiation pressure. The a priori uncertainty on all parameters has been selected sufficiently large so as not to constrain the estimate. The a priori on $\gamma$ and $\beta$ is set to 1, while that on the Lense–Thirring effect is set to be 100%. The only exception is the a priori uncertainty on empirical accelerations, which has instead been set to $5 \times 10^{-8}\,\mathrm{m\,s^{-2}}$ with a time update of 4 minutes, resulting in more parameters than that used in Durante et al. (2020; where the a priori was $2 \times 10^{-8}\,\mathrm{m\,s^{-2}}$ with a time update of 10 minutes), which is one of the best options found by Durante et al. (2022; see its supporting information) to fit the data with an empirical acceleration model. Note that if we either use lower a priori uncertainties or larger time updates, the data fit starts degrading, and residual signatures appear in Doppler data close to the perijove time in given passes.

## 4. Results

The results obtained for the two PPN parameters $\gamma$ and $\beta$ as well as for the Lense–Thirring effect are given in Table 1. We also report the case in which the $\gamma$ parameter is estimated only from the relativistic time delay effect. This is achieved by not including the contribution to observables partial derivatives from the spacecraft dynamics, while accounting for its effect during trajectory integration. Results show that the estimate of $\gamma$ is driven by its effect on the light-time computation, whereas the contribution to the final accuracy from the spacecraft dynamics is negligible, as indicated also by the pretty poor accuracy obtained for $\beta$, which does not affect the radio signal propagation. Results for the $\gamma$ parameter are also given in Figure 3, which shows a comparison of our results with previous works.

Concerning the Lense–Thirring, the effect is too small to provide a reliable estimate of the phenomenon at Jupiter with Juno Doppler data. Additionally, the data fit shows a large correlation with the orientation of Jupiter pole (for a complete discussion see Serra et al. 2016), which precludes an accurate estimate of the effect with Juno. Results indicate that the accuracy is pretty poor: 67% of the total effect at $1\sigma$ (close to the a priori uncertainty set at 100%). The estimated value is indeed compatible with general relativity predictions.

Note that the presented result is compatible, within $1\sigma$, with solutions obtained by either changing the a priori uncertainty on empirical acceleration (from $1 \times 10^{-7}$ to $2 \times 10^{-8}\,\mathrm{m\,s^{-2}}$) or by changing their time update (from 3 to 10 minutes), even if the data fit might be degraded. This is also an indication that the relativity parameters are not correlated with the empirical accelerations required to fit the data.

## 5. Conclusions

In this work, we analyzed Juno Doppler data to perform tests of general relativity at Jupiter. Results show that the values for the estimated parameters are compatible with general relativity predictions, although Juno data have shown poor sensitivity to $\beta$ and the Lense–Thirring effect, since the effect on Juno dynamics is small. The accuracy on the $\gamma$ parameter (controlling both the propagation of the spacecraft trajectory and the light-time computation) has been shown to be driven by the light-time deflection on radio signal propagation, not by its contribution to the dynamics. Although the Cassini solar conjunction experiment provided a more accurate determination of this parameter (Bertotti et al. 2003), the deflection of radio signals was caused by the spacetime curvature induced by the large mass of the Sun. On the contrary, our analysis measured general relativistic effects on a radio signal propagation caused by Jupiter's mass, thus in an environment significantly different from that of solar conjunction experiments. In this work, we obtain an accuracy $\sim$7 times better than previous experiments that used Jupiter as the mass causing spacetime deformation (see Fomalont & Kopeikin 2007; Li et al. 2022), further confirming general relativity predictions around Jupiter.

## Acknowledgments

This work has been supported in part by the Italian Space Agency under agreement No. 2022-16-HH.0. Part of this research was carried out in part at the Jet Propulsion Laboratory, California Institute of Technology, under a contract with the National Aeronautics and Space Administration.

## Data Availability

The raw tracking data and calibration files used in the analysis are available through NASA's Planetary Data System (Buccino 2016). The geometry of the Juno orbit, including SPK

trajectory files and CK spacecraft attitude files, as well as Jupiter satellite ephemeris (jup380) are available at https://naif.jpl.nasa.gov/pub/naif/JUNO/kernels/.

## ORCID iDs

Daniele Durante https://orcid.org/0000-0002-7888-3021
P. Cappuccio https://orcid.org/0000-0002-8758-6627
I. di Stefano https://orcid.org/0000-0003-1491-6848
M. Zannoni https://orcid.org/0000-0002-4151-9656
L. Gomez Casajus https://orcid.org/0000-0002-7972-4006
G. Lari https://orcid.org/0000-0003-0868-8498
D. R. Buccino https://orcid.org/0000-0002-2888-5918
L. Iess https://orcid.org/0000-0002-6230-5825
R. S. Park https://orcid.org/0000-0001-9896-4585
S. J. Bolton https://orcid.org/0000-0002-9115-0789

## References

Anderson, J. D., Esposito, P. B., Martin, W., Thornton, C. L., & Muhleman, D. O. 1975, ApJ, 200, 221
Bertotti, B., Iess, L., & Tortora, P. 2003, Natur, 425, 374
Bolton, S. J., Adriani, A., Adumitroaie, V., et al. 2017, Sci, 356, 821
Buccino, D. R. 2016, Juno Outer Cruise Raw Gravity Science V1.0, NASA PDS, doi:10.17189/MKAT-JH51
Buccino, D. R., Kahan, D. S., Parisi, M., et al. 2021, RaSc, 56, e2021RS007387
Cappuccio, P., Di Stefano, I., Cascioli, G., & Iess, L. 2021, CQGra, 38, 22
Ciufolini, I., Kopeikin, S., Mashhoon, B., & Ricci, F. 2003, PhLA, 308, 101
Ciufolini, I., Paolozzi, A., Pavlis, E. C., et al. 2019, EPJC, 79, 872
Ciufolini, I., Paris, C., Pavlis, E. C., et al. 2023, EPJP, 138, 1054
Ciufolini, I., & Pavlis, E. C. 2004, Natur, 431, 958
di Stefano, I., Cappuccio, P., Di Benedetto, M., & Iess, L. 2022, AdSpR, 70, 854
di Stefano, I., Cappuccio, P., & Iess, L. 2021, CQGra, 38, 055002
Durante, D., Guillot, T., Iess, L., et al. 2022, NatCo, 13, 4632
Durante, D., Parisi, M., Serra, D., et al. 2020, GeoRL, 47, e86572
Einstein, A. 1915, SPAW, 844
Einstein, A. 1916, AnP, 354, 769
Evans, S., Taber, W., Drain, T., et al. 2018, CEAS, 10, 79
Fienga, A., Laskar, J., Exertier, P., Manche, H., & Gastineau, M. 2015, CeMDA, 123, 325
Folkner, W. M., Iess, L., Anderson, J. D., et al. 2017, GeoRL, 44, 4694
Fomalont, E. B., & Kopeikin, S. M. 2003, ApJ, 598, 704
Fomalont, E. B., & Kopeikin, S. M. 2008, in Proc. IAU Symp. 248, A Giant Step: from Milli- to Micro-arcsecond Astrometry, ed. W. J. Jin, I. Platais, & M. A. C. Perryman, 383
Helled, R., Anderson, J. D., Shubert, G., & Stevenson, D. J. 2011, Icar, 216, 440
Iess, L., Asmar, S. W., Cappuccio, P., et al. 2021, SSRv, 217, 21
Iess, L., Folkner, W. M., Durante, D., et al. 2018, Natur, 555, 220
Iorio, L., Girija, A. P., & Durante, D. 2023, MNRAS, 523, 3595
Kaspi, Y., Galanti, E., Park, R. S., et al. 2023, NatAs, 7, 1463
Lari, G., Schettino, G., Serra, D., & Tommei, G. 2022, ExA, 53, 159
Lari, G., Zannoni, M., Durante, D., Park, R., & Tommei, G. 2024, Aeros, 11, 124
Le Poncin-Lafitte, C., & Teyssandier, P. 2008, PhRvD, 77, 044029
Lense, J., & Thirring, H. 1918, PhyZ, 19, 156
Li, Y., Xu, Y., Li, J., et al. 2022, ApJ, 925, 47
Mariotti, G., & Tortora, P. 2013, RaSc, 48, 111
Militzer, B., & Hubbard, W. B. 2023, PSJ, 4, 95
Moyer, T. D. 2008, Formulation for Observed and Computed Values of Deep Space Network Data Types for Navigation (New York: Wiley)
Notaro, V., Durante, D., Iess, L., & Bolton, S. 2021, JGCD, 44, 1062
Parisi, M., Kaspi, Y., Galanti, E., et al. 2021, Sci, 374, 964
Park, R. S., Folkner, W. M., Konopliv, A. S., et al. 2017, AJ, 153, 121
Park, R. S., Folkner, W. M., Williams, J. G., & Boggs, D. H. 2021, AJ, 161, 105
Reasenberg, R. D., Shapiro, I. I., MacNeil, P. E., et al. 1979, ApJ, 234, 219
Serra, D., Dimare, L., Tommei, G., & Milani, A. 2016, P&SS, 134, 100
Serra, D., Lari, G., Tommei, G., et al. 2019, MNRAS, 490, 766
Shapiro, I. I. 1964, PhRvL, 13, 789
Shapiro, I. I., Ash, M. E., & Ingalls, R. P. 1971, PhRvL, 26, 1132
Shapiro, I. I., Pettengill, G. H., & Ash, M. E. 1968, PhRvL, 20, 1265
Soffel, M., Wirrer, R., Schastok, J., Ruder, H., & Schneider, M. 1988, CeMec, 42, 81
Tommei, G., Dimare, L., Serra, D., & Milani, A. 2015, MNRAS, 446, 3089
Will, C. M. 2014, LRR, 17, 4
Will, C. M. 2018, Theory and Experiment in Gravitational Physics (2nd ed.; Cambridge: Cambridge Univ. Press)